AJNR

Neurovascular Imaging with Ultra-High-Resolution Photon-Counting CT: Preliminary Findings on Image-Quality Evaluation

Adrienn Tóth, Justin A. Chetta, Milad Yazdani, M. Gisele Matheus, Jim O'Doherty, Sameer V. Tipnis and M. Vittoria Spampinato

Neurovascular Imaging with Ultra-High-Resolution Photon-Counting CT: Preliminary Findings on Image-Quality Evaluation

Adrienn Tóth, Justin A. Chetta, Milad Yazdani, M. Gisele Matheus, Jim O'Doherty, Sameer V. Tipnis, and M. Vittoria Spampinato

ABSTRACT

BACKGROUND AND PURPOSE: The first-generation photon-counting detector CT was recently introduced into clinical practice and represents a promising innovation in high-resolution CT imaging. The purpose of this study was to assess the image quality of ultra-high-resolution photon-counting detector CT compared with energy-integrating detector CT and to explore different reconstruction kernel sharpness levels for the evaluation of intracranial aneurysms.

MATERIALS AND METHODS: Ten patients with intracranial saccular aneurysms who had previously undergone conventional energy-integrating detector CT were prospectively enrolled. CT angiograms were acquired on a clinical dual-source photon-counting detector CT in ultra-high-resolution mode and reconstructed with 4 vascular kernels (Bv36, Bv40, Bv44, Bv48). Quantitative and qualitative image-quality parameters of the intracranial arteries were evaluated. For the quantitative analysis (image noise, SNR, contrast-to-noise ratio), ROIs were manually placed at standard anatomic intracranial and extracranial locations by 1 author. In addition, vessel border sharpness was evaluated quantitatively. For the qualitative analysis, 3 blinded neuroradiologists rated photon-counting detector CT and energy-integrating detector CT image quality for the evaluation of the intracranial vessels (ie, the aneurysms and 9 standard vascular branching locations) on a 5-point Likert-type scale. Additionally, readers independently selected their preferred kernel among the 4 kernels evaluated on photon-counting detector CT.

RESULTS: In terms of quantitative image quality, Bv48, the sharpest kernel, yielded increased image noise and decreased SNR and contrast-to-noise ratio parameters compared with Bv36, the smoothest kernel. Compared with energy-integrating detector CT, the Bv48 kernel offered better quantitative image quality for the evaluation of small intracranial vessels ($P < .001$). Image-quality ratings of the Bv48 were superior to those of the energy-integrating detector CT and not significantly different from ratings of the B44 reconstruction kernel. When comparing side by side all 4 photon-counting detector reconstruction kernels, readers selected the B48 kernel as the best to visualize the aneurysms in 80% of cases.

CONCLUSIONS: Ultra-high-resolution photon-counting detector CT provides improved image quality for neurovascular imaging. Although the less sharp kernels provided superior SNR and contrast-to-noise ratio, the sharpest kernels delivered the best subjective image quality on photon-counting detector CT for the evaluation of intracranial aneurysms.

ABBREVIATIONS: AcomA = anterior communicating artery; Bv = body vascular; CNR = contrast-to-noise ratio; CTDI$_{vol}$ = CT dose index volume; EID = energy-integrating detector; OA = ophthalmic arteries; PCD = photon-counting detector; PcomA = posterior communicating artery; QIR = quantum iterative reconstruction; SOC = standard of care; UHR = ultra-high-resolution; VB = vertebral artery–basilar artery junctions

CTA is routinely performed to evaluate intracranial aneurysms with high reported sensitivity and specificity.[1-5] However, the

spatial resolution of conventional CT (energy-integrating detector [EID]) is not always adequate to fully characterize small aneurysms (≤3 mm) and may have limitations in differentiating a tortuous vessel or infundibulum from an aneurysm.[6] The recent introduction of photon-counting detectors (PCDs) is a breakthrough in CT technology. Conventional EIDs convert the incoming x-ray photons into visible light, which is then converted into an electrical signal. Instead, PCDs omit the light scintillation step and directly generate electrical signal proportional to the energy of an incoming x-ray. This process results in the measurement of the energy of the incident photons, thus enabling multienergy imaging.[7-9] With currently available whole-body

SUMMARY

PREVIOUS LITERATURE: Sharper reconstruction kernels in CT angiography can enhance spatial frequencies and image detail similar to 3D angiography, showing promise for improving clinical decision-making by providing more accurate anatomic characterization of intracranial aneurysms. While previous studies have evaluated ultra-high-resolution photon-counting CT for coronary angiography and recommended optimal kernel selection, there is a lack of literature on its use in neurovascular imaging.

KEY FINDINGS: The use of the Bv48 kernel significantly improved vessel sharpness, especially in smaller intracranial arteries. The 3 readers of the study favored the sharper kernels for the visualization of saccular aneurysms. UHR PCD-CT images significantly improved vessel sharpness and subjective image quality compared with standard EID-CT.

KNOWLEDGE ADVANCEMENT: This study provides an initial evaluation of quantitative and qualitative image quality by using different reconstruction kernels in a selected group of patients with intracranial saccular aneurysms. Our preliminary results could lay the foundation for future studies and help guide protocol optimization for neurovascular imaging on PCD-CT.

clinical PCD-CT systems, ultra-high-resolution (UHR) imaging is available with a detector pixel size of 0.151 × 0.176 mm^2 at the isocenter, offering a maximum in-plane image resolution of 0.11 mm and a maximum through-plane resolution of 0.16 mm.[10] These technical innovations allow improved soft-tissue and iodine contrast, improved spatial resolution, decreased image noise, and reduced beam-hardening and metal-associated artifacts.[11-15]

We hypothesized that the enhanced image quality of UHR PCD-CT may facilitate the detailed characterization of intracranial aneurysms. The selection of the reconstruction kernel is a key aspect of image-postprocessing that requires careful consideration, because it frequently involves striking a balance between enhanced spatial resolution and image noise.[16,17] As for the detailed anatomic characterization of intracranial aneurysms, sharper kernels may provide more accurate information than smooth CT kernels.[18] In the present study, we aimed to assess the image quality of UHR PCD-CT compared with EID-CT and to explore different reconstruction kernel sharpness levels for the evaluation of intracranial aneurysms.

MATERIALS AND METHODS

Study Population
This prospective, single-center study was approved by the institutional review board of the Medical University of South Carolina, and written informed consent was obtained from all participants. We enrolled consecutive patients between July and September 2023 who met the following criteria: 18 years of age or older, prior clinically-indicated standard of care (SOC) CTA of the head and neck on EID-CT within the previous 8 months, and 1 or multiple untreated intracranial saccular aneurysms. Exclusion criteria included a history of iodine contrast allergy, renal insufficiency, pregnancy, nondiagnostic SOC CTA, and scheduled neurovascular surgery (endovascular coiling or clipping). After the initial screening, the senior author reviewed each CT angiogram to confirm eligibility for the study. If it was unclear whether the patient had a saccular aneurysm or an infundibulum, then the patient was excluded from the study.

PCD-CT Image Acquisition and Reconstruction
Patients underwent head and neck CTA acquired on a clinical first-generation PCD-CT scanner (NAEOTOM Alpha; Siemens) operated in Quantum HD UHR mode, resulting in a collimation of 120 × 0.2 mm at the detector level and a reconstructed section thickness of 0.2 mm. The reconstructed matrix size was 512 × 512, and the field of view was adjusted for each patient to optimally image the vessels from the aortic arch to the vertex. We used the following acquisition parameters: tube voltage = 140 kV(peak), pitch = 0.65, rotation time = 0.5 seconds. To achieve a comparable absorbed radiation dose between scans, we used the CT dose index volume (CTDI$_{vol}$) from the EID-CT scan of each patient as a reference. The tube current–time product (milliampere-seconds) of the PCD-CT scan was adjusted to match the reference CTDI$_{vol}$.

CTA was performed after the administration of 80 mL of iodinated contrast material (iohexol, Omnipaque 350; GE Healthcare), injected through a 20-ga IV antecubital vein catheter using a power injector. The flow rate was matched to the EID-CT scan per patient, with an average of 4.37 (SD, 0.5) mL/s. Opacification of the aortic arch was monitored using a bolus-tracking technique with an attenuation threshold of 155 HU for all examinations. The start time of data acquisition was determined with a fixed delay of 5 seconds after the attenuation threshold was reached.

Axial plane, polyenergetic images (referred to as T3D by the manufacturer) were reconstructed at 0.2-mm section thickness with a 0.2-mm section increment. Quantum iterative reconstruction (referred to as QIR by the manufacturer) level 1 was used for all PCD-CT images. Four image sets were reconstructed using the following vascular kernels: body vascular [Bv]36 (least sharp, representing the standard clinical reconstruction kernel used for head and neck CTA in our institution), Bv40, Bv44, and Bv48 (Online Supplemental Data).

Quantitative Analysis
Quantitative image analysis was performed by 1 author (A.T.) using a manufacturer-specific workstation (syngo.via software version VB30; Siemens). ROIs were manually placed on 1 PCD-CT reconstruction (Bv36) at 12 standard anatomic locations, bilaterally. ROIs were copied and pasted onto the other 3 reconstructions, placing the ROIs at the exact same location with the exact same size on every PCD-CT reconstruction. The ROIs on the EID-CT images were closely matched (manually) in both size and location to the PCD-CT image sets on a per-patient basis. The data analysis used the average of the 2 bilateral ROIs at each location.

Attenuation was measured in 3 extracranial vessels: the common carotid artery, the cervical ICA (C1), and the cervical vertebral artery (V2). We selected 7 intracranial locations: the petrous segment of the ICA (C2), the carotid terminus, MCA (M1), anterior cerebral artery (A2), posterior cerebral artery (P2), intradural vertebral artery (V4), and the basilar artery. The size of the ROIs was as large as possible, ensuring that only the contrasted lumen of the artery was measured. Intracranial vessel measurements were divided into 2 groups based on the size of the ROIs: The first comprised large intracranial vessels including C2 and carotid terminus (mean ROI area = 4.28 [SD, 2.02] and 2.39 [SD, 0.74] mm^2, respectively), while the second consisted of small intracranial vessels such as M1, A2, P2, V4, and the basilar artery (mean ROI area ranged from 0.70 [SD, 0.20] mm^2 to 1.53 [SD, 0.36] mm^2). Results from the analysis of the combined groups were reported.

Signal was defined as the average density (Hounsfield units); and noise, as the SD of density within the voxels of the ROIs. For the calculation of the SNR and contrast-to-noise ratio (CNR), the muscle density in the pterygoid muscle and the SD of the air adjacent to the neurocranium were measured (both ROI areas: 0.25 cm^2). The SNR and CNR were calculated as follows:

$$SNR = \frac{signal_{artery}}{SD_{artery}}.$$

$$CNR = \frac{signal_{artery} - signal_{muscle}}{SD_{air}}.$$

Additionally, images were transferred to a dedicated workstation (ImageJ software, Version 1.53; National Institutes of Health) to analyze the sharpness of vessel borders.[17,19,20] For each image, a total of 6 line profiles were placed perpendicular to the border of the vessels to detect attenuation values at the following locations: C1 and V2 (representing the extracranial arteries), C2 and carotid terminus (representing the large intracranial arteries), M1 and A2 (representing the small intracranial arteries). For each line, the maximum per-pixel change in signal intensity (maximum ΔHU) and the full width at half maximum was calculated. Vessel sharpness was defined as the mean maximum change of CT values.

Qualitative Analysis
Qualitative image quality was assessed by 3 experienced neuroradiologists (J.A.C., M.G.M., and M.Y.). Image analysis was performed using the in-house PACS system. A training session was conducted with the readers before the image rating, and reference images were provided to ensure consistency and facilitate the application of the rating scale. The readers independently rated the images at the following intracranial locations: right and left ICA (C2 segment), PICA, vertebral artery–basilar artery junctions (VB), ophthalmic arteries (OA), carotid terminus, posterior communicating artery (PcomA), MCA trifurcation, anterior communicating artery (AcomA), basilar artery apex, and at the location of the aneurysm/s. In the first part of the evaluation, PCD-CT reconstructions and EID-CT images were displayed one by one sequentially in a randomized order, while readers were asked to rate the image quality using a 5-point Likert-type scale (Online Supplemental Data). Images were initially shown at

predefined window settings (width: 1500 HU; level: 400 HU), but the readers were allowed to perform manual adjustments. Next, the 4 PCD-CT reconstructions of each patient were displayed on 1 monitor in a randomized order, and readers were asked to choose the most suitable for the evaluation of the intracranial aneurysm/s. Readers were blinded to the type of reconstructions and scanner type at each step of the image evaluation.

Statistical Analysis
Patient and examination characteristics were summarized descriptively. The normality of distributions was assessed using histograms and the Shapiro-Wilk test. The 2-sided Wilcoxon signed-rank test was used to assess differences in the distribution of qualitative and non-normally distributed quantitative image-quality scores. Scores from the qualitative image-quality analysis were pooled across readers. The interreader agreement of qualitative scores among the 3 readers was quantified with Krippendorf α coefficients (α = 0.0–0.20, poor agreement; α = 0.21–0.40, fair agreement; α = 0.41–0.60, moderate agreement; α = 0.61–0.80, substantial agreement; α = 0.81–1.00, almost perfect agreement). All P values were corrected for multiple testing using the Bonferroni correction. Two-tailed P values < .05 were considered statistically significant. If not stated otherwise, all data are presented as mean (SD). All statistical analyses were performed by using SPSS, Version 28.0.1 (IBM).

RESULTS
Patient Population and Radiation Dose Parameters
Sample images are provided in Fig 1. The study population included 10 patients, and 8 were women. The mean age at the time of the second (PCD-CT) scan was 59.5 (SD, 18.3) years. The indications of the SOC CTA included aneurysm follow-up or sudden headache with a history of an intracranial aneurysm (n = 6), clinical suspicion of acute stroke (n = 2), head trauma (n = 1), and dizziness (n = 1). A total of 13 intracranial aneurysms were detected at the following locations: ICA (n = 5), MCA (n = 4), AcomA (n = 2), and PcomA (n = 2), with an average maximum diameter of 3.5 (SD, 1.5) mm (Online Supplemental Data). The radiation dose parameters for the EID-CT and PCD-CT examinations were as follows: CTDI$_{vol}$ = 22.55 (SD, 12.16) mGy, dose-length product = 695.35 (SD, 288.58) mGy*cm, effective milliampere-seconds = 270.22 (SD, 55.65) and CTDI$_{vol}$ = 18.87 (SD, 3.03) mGy, dose-length product = 695.50 (SD, 127.03) mGy*cm, effective milliampere-seconds = 175.70 (SD, 35.36), respectively.

Quantitative Analysis: PCD-CT Reconstructions
An incremental increase in mean attenuation was found across the range of kernels, transitioning from the smoothest (Bv36) to the sharpest (Bv48) kernel in the extracranial (from 516.13 [SD, 108.1] to 521.92 [SD, 108.53], respectively) and large intracranial (from 476.88 [SD, 104.70] to 489.38 [SD, 106.88], respectively) locations, and a more pronounced increase was evident in the small intracranial arteries (from 425.74 [SD, 91.21] to 482.23 [SD, 110.89], respectively) (all from P < .001 to P = .048). Image noise significantly increased from Bv36 to Bv48, with the highest increase measured at the large intracranial vessels (from 10.70
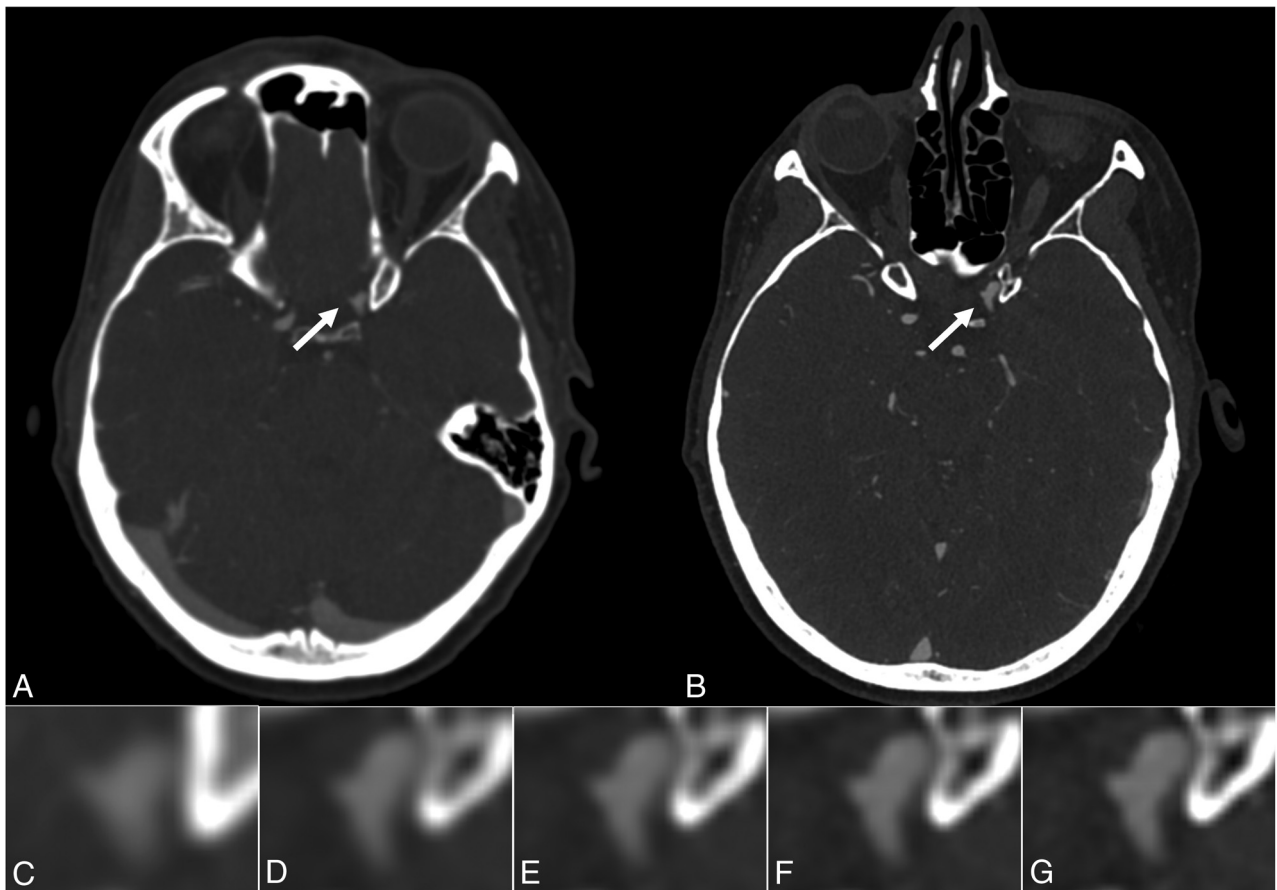
FIG 1. A 44-year-old woman with a saccular intracranial aneurysm. EID-CT (*A* and *C*) and UHR PCD-CT (*B, D–G*) angiograms of the head show an intracranial saccular aneurysm of the left paraclinoid ICA (*arrows*). PCD-CT reconstructions show increasing vessel sharpness with higher kernel levels: *D*, (Bv36). *E*, (Bv40). *F*, (Bv44). *G*, (Bv48). Window settings were identical in each image.
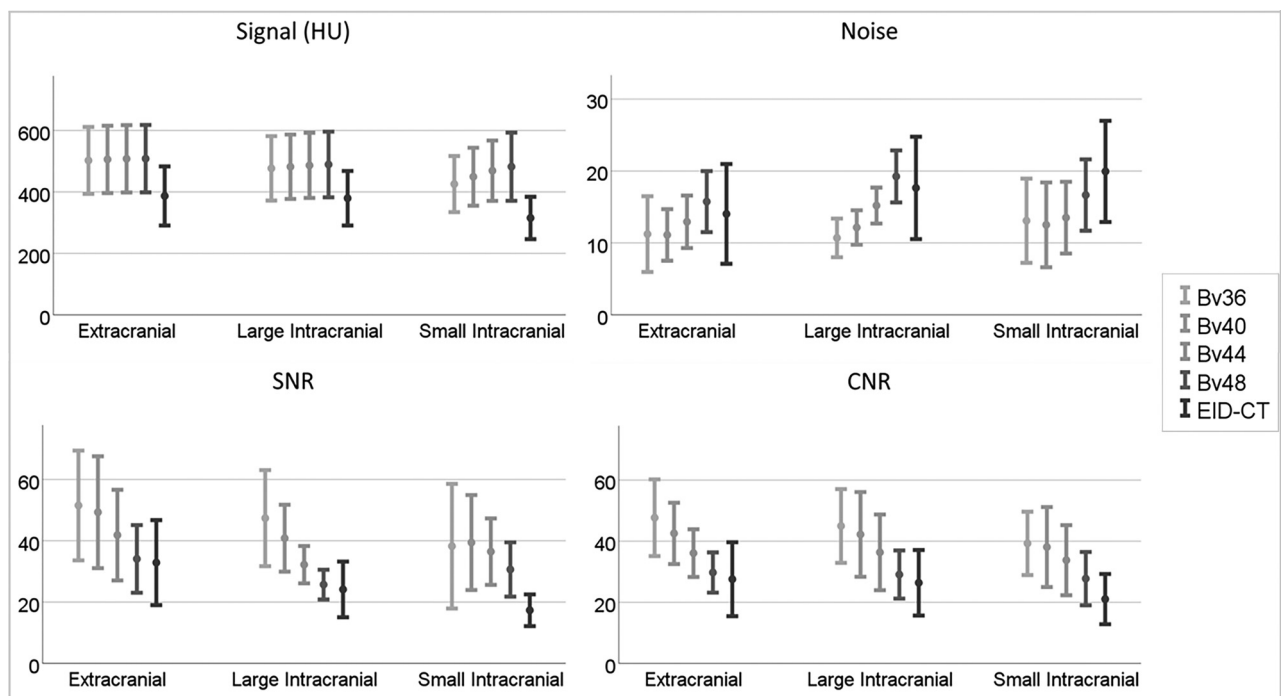

FIG 2. Quantitative image-quality analysis. Signal, noise, SNR, and CNR scores of the PCD-CT (Bv36, Bv40, Bv44, Bv48) and EID-CT images are represented with *error bars* (mean [SD]).
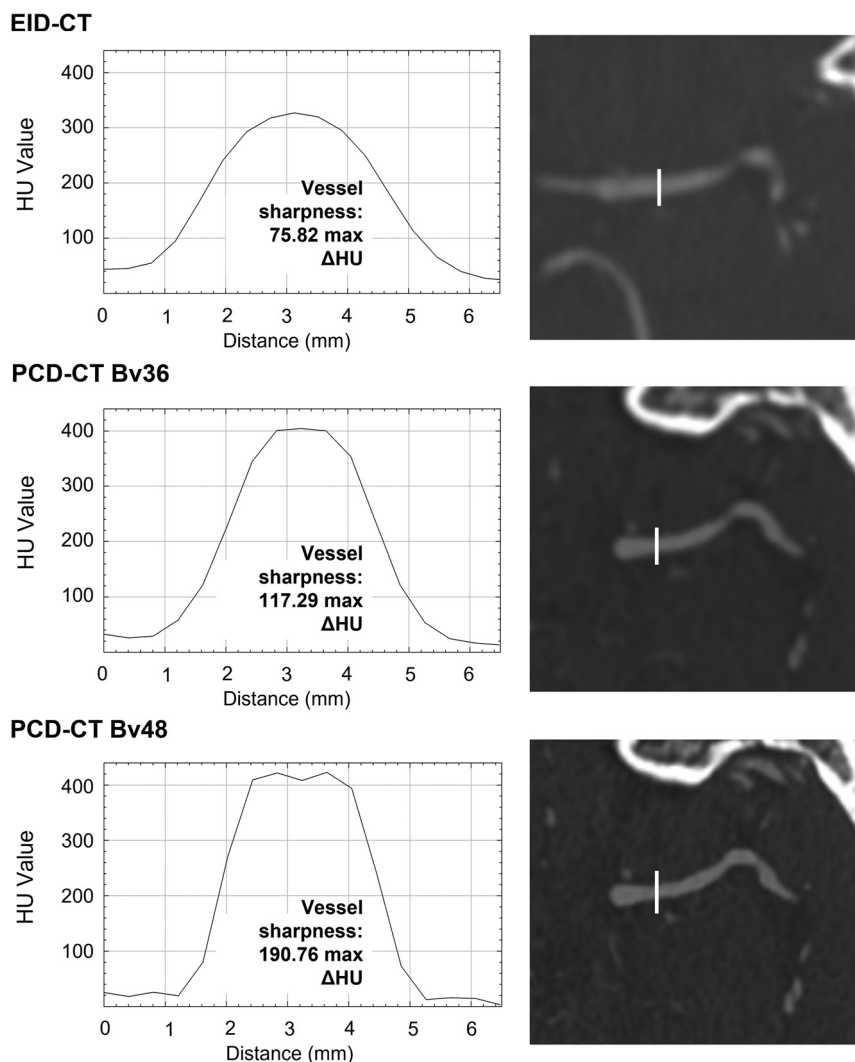
EID-CT

PCD-CT Bv36

PCD-CT Bv48

FIG 3. Example of vessels sharpness measurements. *Line profiles* of the MCA and corresponding images: EID-CT (*upper row*), PCD-CT Bv36 (*middle row*), PCD-CT Bv48 (*lower row*). A steeper slope representing a sharper vessel wall can be observed in the Bv48 image (vessel sharpness = 217.8 maximum ΔHU), compared with the Bv36 (vessel sharpness = 139.8 maximum ΔHU) and the EID-CT image (vessel sharpness = 102.6 maximum ΔHU).

[SD, 2.69] to 19.25 [SD, 3.62], $P < .001$). The least sharp kernel (Bv36) provided the highest SNR and CNR, mostly with significant differences compared with the sharpest (Bv48) kernel (from $P < .001$ to $P = .228$). Vessel sharpness increased with higher kernel levels ($P < .001$), with the greatest difference observed in small intracranial vessels (from 139.87 [SD, 31.23] to 221.69 [SD, 49.46]).

Quantitative Analysis: PCD-CT versus EID-CT
Quantitative image quality measures from EID-CT and PCD-CT (Bv48) were compared. Vascular attenuation as measured on PCD-CT reconstructions was significantly higher than that of EID-CT at each location (from $P < .001$ to $P = .004$). While there was no statistically significant difference in image noise between the PCD-CT Bv48 images and EID-CT at the extracranial and large intracranial locations ($P = .224$ and $P = .646$, respectively), the Bv48 reconstruction exhibited significantly lower image noise in the small intracranial arteries (16.66 [SD, 4.96] versus 19.95

[SD, 7.04], $P = .012$). In terms of SNR and CNR, PCD-CT outperformed the EID-CT images at every location, with a statistically significant difference at the small intracranial arteries (30.65 [SD, 8.86] and 27.76 [SD, 8.71] versus 17.34 [SD, 5.17] and 21.06 [SD, 8.22], respectively, all $P < .001$). Vessel sharpness was significantly higher for PCD-CT than for EID-CT ($P < .001$). Detailed results are provided in Online Supplemental Data and Figs 2–3.

Qualitative Analysis
Moderate agreement ($\alpha = 0.50$) was found among the 3 readers for qualitative ratings using the 5-point Likert-type scale. The qualitative analysis revealed the superiority of PCD-CT (Bv48) over EID-CT at each intracranial location (all $P < .001$). Images reconstructed with either the Bv44 or the Bv48 kernel achieved the highest scores (Online Supplemental Data and Fig 4). However, the difference between Bv44 and Bv48 was not statistically significant ($P = .166–1.00$). When we reviewed the PCD-CT images side by side, the Bv48 reconstruction was selected as the most suitable for the evaluation of intracranial aneurysms by the readers in 80% of cases, while Bv44 was chosen in 20% of cases.

DISCUSSION
The present study evaluated the objective and subjective image quality of UHR PCD-CTA for neurovascular imaging using different levels of kernel sharpness in patients with intracranial saccular aneurysms. Our results highlight the significance of sharper kernels in enhancing the characterization of intracranial aneurysms. The use of the Bv48 kernel significantly increased vessel sharpness, especially of the small intracranial arteries. Our analysis included a comparison of PCD-CT and EID-CT images, confirming previous findings that PCD-CT offers superior image quality for neurovascular imaging.[21,22] Objectively, UHR (0.2 mm) PCD-CT images significantly increased vessel sharpness and provided improved subjective image quality compared with the SOC EID-CT. Of the 4 reconstruction kernels evaluated on PCD-CT, the 3 readers of the study favored the sharpest reconstruction kernel for the visualization of saccular aneurysms. Although radiation-dose reduction was not the primary focus of this study, our results suggest that improved image quality may be achievable with PCD-CT at a significantly reduced radiation dose compared with EID-CT.

The recent introduction of photon-counting CT into clinical practice promises significant advantages over EID-CT in many
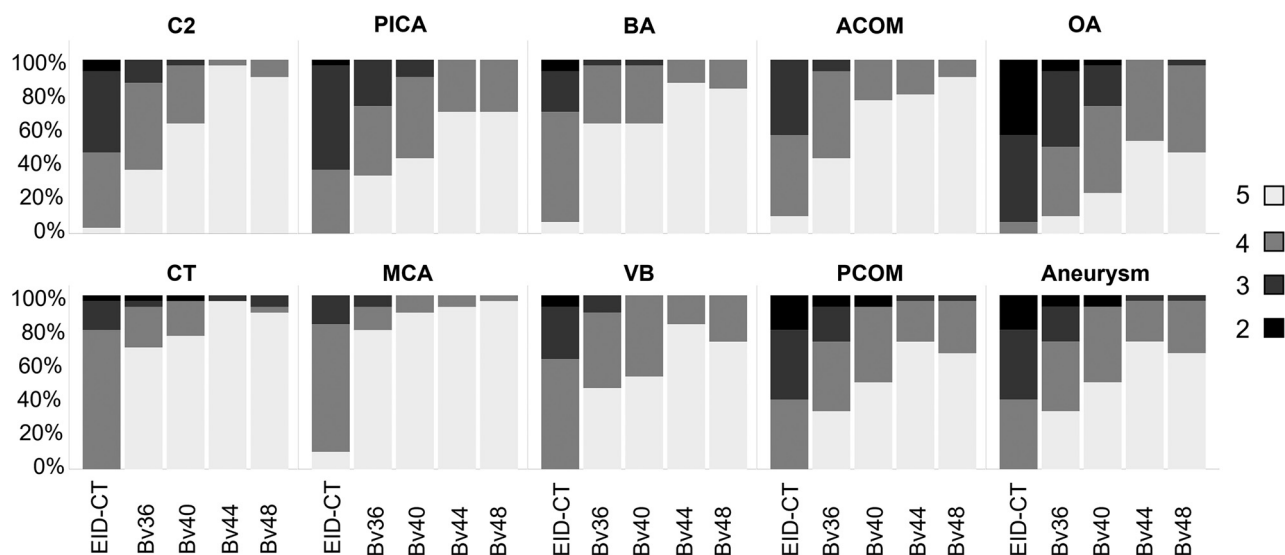
FIG 4. Qualitative image-quality scores from the EID-CT and PCD-CT CT (Bv36, Bv40, Bv44, Bv48) images. Stacked *bar charts* show the pooled ratings from 3 readers in percentages. The 10 evaluated intracranial locations are the following: ICA (C2 segment), PICA, basilar artery (BA), AcomA, OA, carotid terminus (CT), MCA, VB, PcomA and the location of the aneurysm/s. Interpretation of scores: 5 = excellent image quality, 4 = good image quality, 3 = acceptable image quality, 2 = barely satisfactory image quality, 1 = unacceptable image quality.

diagnostic fields because it offers precise visualization of small anatomic structures and depiction of subtle pathologic changes.[23-26] Moreover, improved lumen visualization and plaque imaging have been reported in various in vitro and in vivo studies, commonly in coronary imaging.[19,27] As for neurovascular imaging, the image quality of PCD-CTA has been shown to be excellent using polyenergetic as well as monoenergetic reconstructions.[28,29]

Related literature on kernel optimization for intracranial aneurysm imaging has been limited to EID-CT platforms. O'meara et al[18] showed that higher spatial frequencies and greater image details are more comparable with 3D rotational angiography using a sharp reconstruction kernel (H60f) in contrast to a smooth kernel (H20f). They report that using a sharper kernel can improve image resolution but may also increase image noise. Nevertheless, this use can lead to improved decision-making ability and clinical utility of CTA, by providing more accurate anatomic characterization of intracranial aneurysms. Yang et al[30] evaluated the image quality of coronary CT angiography using PCD-CT with 4 kernel sharpness levels (36/40/44/48) across 3 different kernel types (Br/Bv/Qr). On the basis of their objective and subjective image-quality results, the authors recommended the use of Bv40 for spectral PCD-CT coronary angiography applications. Image quality of PCD-CT for neurovascular applications across different kernel reconstructions requires further determination.

To the best of our knowledge, the present study represents the first systematic assessment of image quality across different reconstruction kernels for neurovascular imaging using PCD-CT. Our preliminary results provide quantitative and qualitative image-quality measures of UHR PCD-CT imaging in a selected group of patients with intracranial saccular aneurysms. Our quantitative analysis yielded predictable results, showing that image noise increases using sharper kernels, resulting in a continuous decrease in SNR and CNR. Nevertheless, our qualitative image-quality analysis demonstrated a clear preference of the

readers for the sharpest kernels, outperforming the other PCD-CT reconstructions, as well as the SOC EID-CT images. The comparison of EID-CT with the Bv48 PCD-CT images revealed that while the Bv48 kernel performs less favorably in quantitative terms compared with other PCD-CT reconstructions, it still demonstrates comparable or superior performance over EID-CT. The use of quantitative measures, such as signal, noise, SNR, and CNR, offers a robust framework for assessing image quality. However, for a comprehensive evaluation of image quality, both qualitative and qualitative assessments should be considered, because they provide complementary information.

When in disagreement, the authors of this article argue that qualitative evaluation may outweigh quantitative evaluation. The Bv44 and Bv48 kernels both delivered superior qualitative image quality. However, the observers favored the Bv48 reconstructions kernel for evaluating the relatively small-sized aneurysms identified in the study cohort, likely due to the improved vessel sharpness, notably observed in the small intracranial arteries.

Intracranial vessel visualization with state-of-the-art EID-CT technology provides good image quality and enables the correct visualization of intracranial aneurysms but usually has limitations in visualizing smaller aneurysms. While DSA remains the criterion standard test for the detection and characterization of intracranial aneurysms, UHR PCD-CT has the potential to offer less invasive imaging, even for small intracranial aneurysms, with a significantly reduced radiation dose. Our preliminary results may provide a valuable reference to exploit the full potential of the UHR mode of head and neck PCD-CT.

The limitations of our study merit consideration. First, this preliminary study included a very small number (*n* = 10) of patients from a single center, limiting the generalizability of our results. Second, only 1 type of kernel (Bv) and 4 levels of kernel sharpness (36, 40, 44, 48) were evaluated on PCD-CT. The Bv is the kernel type routinely used in our institution for head and neck CTA. Because we aimed to compare the image quality of

EID-CT and PCD-CT, we applied a range of reconstruction kernels available on the PCD-CT scanner that are relatively comparable with the reconstruction kernel used for neurovascular EID-CT angiography in clinical practice at our institution. Bv48 is the sharpest kernel evaluated in this study, but it is not the sharpest option available on the PCD-CT. Future studies may investigate the highest, limiting level of kernel sharpness that provides the optimal image quality. Third, we used QIR at strength level 1 for all PCD-CT reconstructions. However, higher QIR levels could potentially compensate for the increase in image noise caused by using sharper kernel levels. Future studies should explore the potential benefits of using sharp kernels in combination with higher QIR levels to achieve improved image quality. Fourth, ROIs were placed manually by a single observer, possibly introducing the risk of measurement bias.

CONCLUSIONS

Our preliminary study shows that UHR PCD-CTA may provide improved image quality for neurovascular imaging applications. A sharper reconstruction kernel seems to be beneficial to achieve optimal image quality for the evaluation of intracranial aneurysms. Further studies are needed to assess the impact of UHR PCD-CT on patient management and outcome.

Disclosure forms provided by the authors are available with the full text and PDF of this article at www.ajnr.org.

REFERENCES

1. Chen X, Liu Y, Tong H, et al. **Meta-analysis of computed tomography angiography versus magnetic resonance angiography for intracranial aneurysm.** *Medicine (Baltimore)* 2018;97:e10771 CrossRef Medline
2. Ni QQ, Chen GZ, Schoepf UJ, et al. **Cerebral CTA with low tube voltage and low contrast material volume for detection of intracranial aneurysms.** *AJNR Am J Neuroradiol* 2016;37:1774–80 CrossRef Medline
3. Menke J, Larsen J, Kallenberg K. **Diagnosing cerebral aneurysms by computed tomographic angiography: meta-analysis.** *Ann Neurol* 2011;69:646–54 CrossRef Medline
4. Westerlaan HE, van Dijk JM, Jansen-van der Weide MC, et al. **Intracranial aneurysms in patients with subarachnoid hemorrhage: CT angiography as a primary examination tool for diagnosis–systematic review and meta-analysis**. *Radiology* 2011;258:134–45 CrossRef Medline
5. Xing W, Chen W, Sheng J, et al. **Sixty-four-row multislice computed tomographic angiography in the diagnosis and characterization of intracranial aneurysms: comparison with 3D rotational angiography.** *World Neurosurg* 2011;76:105–13 CrossRef Medline
6. Luo Z, Wang D, Sun X, et al. **Comparison of the accuracy of subtraction CT angiography performed on 320-detector row volume CT with conventional CT angiography for diagnosis of intracranial aneurysms.** *Eur J Radiol* 2012;81:118–22 Medline
7. Willemink MJ, Persson M, Pourmorteza A, et al. **Photon-counting CT: technical principles and clinical prospects.** *Radiology* 2018;289:293–312 CrossRef Medline
8. Rajendran K, Petersilka M, Henning A, et al. **First clinical photon-counting detector CT system: technical evaluation.** *Radiology* 2022;303:130–38 CrossRef Medline
9. Kreisler B. **Photon counting detectors: concept, technical challenges, and clinical outlook.** *Eur J Radiol* 2022;149:110229 CrossRef Medline
10. Benson JC, Rajendran K, Lane JI, et al. **A new frontier in temporal bone imaging: photon-counting detector CT demonstrates superior visualization of critical anatomic structures at reduced radiation dose.** *AJNR Am J Neuroradiol* 2022;43:579–84 CrossRef Medline
11. Rajagopal JR, Farhadi F, Solomon J, et al. **Comparison of low dose performance of photon-counting and energy integrating CT.** *Acad Radiology* 2021;28:1754–60 CrossRef Medline
12. Pourmorteza A, Symons R, Henning A, et al. **Dose efficiency of quarter-millimeter photon-counting computed tomography: first-in-human results.** *Invest Radiol* 2018;53:365–72 CrossRef Medline
13. Rajagopal JR, Farhadi F, Richards T, et al. **Evaluation of coronary plaques and stents with conventional and photon-counting CT: benefits of high-resolution photon-counting CT.** *Radiol Cardiothorac Imaging* 2021;3:e210102 CrossRef Medline
14. Higashigaito K, Mergen V, Eberhard M, et al. **CT angiography of the aorta using photon-counting detector CT with reduced contrast media volume.** *Radiol Cardiothorac Imaging* 2023;5:e220140 CrossRef Medline
15. Zhou W, Bartlett DJ, Diehn FE, et al. **Reduction of metal artifacts and improvement in dose efficiency using photon counting detector CT and tin filtration.** *Invest Radiol* 2019;54:204–11 CrossRef Medline
16. Milos RI, Röhrich S, Prayer F, et al. **Ultrahigh-resolution photon-counting detector CT of the lungs: association of reconstruction kernel and slice thickness with image quality**. *AJR Am J Roentgenol* 2023;220:672–80 CrossRef Medline
17. von Spiczak J, Mannil M, Peters B, et al. **Photon counting computed tomography with dedicated sharp convolution kernels: tapping the potential of a new technology for stent imaging.** *Invest Radiol* 2018;53:486–94 CrossRef Medline
18. O'meara B, Rahal JP, Lauric A, et al. **Benefit of a sharp computed tomography angiography reconstruction kernel for improved characterization of intracranial aneurysms**. *Neurosurgery* 2014;10(Suppl 1):97–105; discussion 105 CrossRef Medline
19. Mergen V, Sartoretti T, Baer-Beck M, et al. **Ultra-high-resolution coronary CT angiography with photon-counting detector CT: feasibility and image characterization.** *Invest Radiol* 2022;57:780–88 CrossRef Medline
20. Decker JA, O'Doherty J, Schoepf UJ, et al. **Stent imaging on a clinical dual-source photon-counting detector CT system-impact of luminal attenuation and sharp kernels on lumen visibility.** *Eur Radiol* 2023;33:2469–77 CrossRef Medline
21. Symons R, Reich DS, Bagheri M, et al. **Photon-counting computed tomography for vascular imaging of the head and neck: first in vivo human results.** *Invest Radiol* 2018;53:135–42 CrossRef Medline
22. Pourmorteza A, Symons R, Reich DS, et al. **Photon-counting CT of the brain: in vivo human results and image-quality assessment.** *AJNR Am J Neuroradiol* 2017;38:2257–63 CrossRef Medline
23. Gaillandre Y, Duhamel A, Flohr T, et al. **Ultra-high resolution CT imaging of interstitial lung disease: impact of photon-counting CT in 112 patients.** *Eur Radiol* 2023;33:5528–39 CrossRef Medline
24. Prayer F, Kienast P, Strassl A, et al. **Detection of post-COVID-19 lung abnormalities: photon-counting CT versus same-day energy-integrating detector CT.** *Radiology* 2023;307:e222087 CrossRef Medline
25. Sartoretti T, Landsmann A, Nakhostin D, et al. **Quantum iterative reconstruction for abdominal photoncounting detector CT improves image quality.** *Radiology* 2022;304:E55 CrossRef Medline
26. Racine D, Mergen V, Viry A, et al. **Photon-counting detector CT with quantum iterative reconstruction: impact on liver lesion detection and radiation dose reduction.** *Invest Radiol* 2023;58:245–52 CrossRef Medline
27. Si-Mohamed SA, Boccalini S, Lacombe H, et al. **Coronary CT angiography with photon-counting CT: first-in-human results.** *Radiology* 2022;303:303–13 CrossRef Medline

28. Michael AE, Boriesosdick J, Schoenbeck D, et al. **Photon counting CT angiography of the head and neck: image quality assessment of polyenergetic and virtual monoenergetic reconstructions.** *Diagnostics* 2022;12:1306 CrossRef Medline

29. Spampinato MV, Rodgers J, McGill LJ, et al. **Image quality of photon-counting detector CT virtual monoenergetic and polyenergetic** reconstructions for head and neck CT angiography. *Clin Imaging* 2024;108:110081 CrossRef Medline

30. Yang Y, Fink N, Emrich T, et al. **Optimization of kernel type and sharpness level improves objective and subjective image quality for high-pitch photon counting coronary CT angiography.** *Diagnostics (Basel)* 2023;13:1937 CrossRef Medline